IEEE Access
Multidisciplinary ⋮ Rapid Review ⋮ Open Access Journal

Received November 7, 2018, accepted December 4, 2018, date of publication December 10, 2018,
date of current version January 4, 2019.

Digital Object Identifier 10.1109/ACCESS.2018.2885803

Spatiotemporal Adaptive Nonuniformity Correction Based on BTV Regularization

RUI LAI[1], JUNTAO GUAN[1], YINTANG YANG[1], AND AI XIONG[2]
[1]Department of Microelectronics, Xidian University, Xi'an 710071, China
[2]School of Control Engineering, Chengdu University of Information Technology, Chengdu 610103, China

Corresponding author: Rui Lai (rlai@mail.xidian.edu.cn)

This work was supported in part by the Natural Science Foundation of China under Grant 61674120, Grant 61571338, Grant U1709218, and Grant 61672131, in part by the Fundamental Research Funds for the Central Universities of China under Grant JBG161113 and Grant 300102328110, and in part by the Key Research and Development Plan of Shaanxi Province under Grant 2017ZDCXL-GY-05-01.

ABSTRACT The residual nonuniformity response, ghosting artifacts, and over-smooth effects are the main defects of the existing nonuniformity correction (NUC) methods. In this paper, a spatiotemporal feature-based adaptive NUC algorithm with bilateral total variation (BTV) regularization is presented. The primary contributions of the innovative method are embodied in the following aspects: BTV regularizer is introduced to eliminate the nonuniformity response and suppress the ghosting effects. The spatiotemporal adaptive learning rate is presented to further accelerate convergence, remove ghosting artifacts, and avoid over-smooth. Moreover, the random projection-based bilateral filter is proposed to estimate the desired target image more accurately which yields more details in the actual scene. The experimental results validated that the proposed algorithm achieves outstanding performance upon both simulated data and real-world sequence.

INDEX TERMS Infrared imaging, neural networks, image denoising, infrared image sensors.

I. INTRODUCTION

Infrared focal plane array (IRFPA) sensors, being an important front end of internet of things (IOT) [1]–[5], often suffer from the pixel-to-pixel nonuniformity response, which induces fixed pattern noise (FPN) and causes serious decline in image quality [6]–[8]. Nonuniformity correction (NUC), being a cost-effective solution for FPN, is continually investigated and applied nearly all the infrared imaging systems.

Existing NUC algorithms are generally divided into two primary categories: reference-based NUC (RBNUC) and scene-based NUC (SBNUC) algorithm. The RBNUC methods [9] remove the FPN in real time according to the fixed correction parameters that calculated from the response of particular radiation. However, RBNUC methods need to update the correction parameters to compensate the inherent temporal drift of detector characteristics, which will periodically interrupt the normal operation of the imaging system. In view of this, many SBNUC methods have been proposed, such as neural networks (NN) [10]–[12], temporal high-pass filter (THPF) [13]–[15] and constant-statistics (CS) method [16]. Among the SBNUC methods, the NN-NUC is a representative approach with balanced precision and computational load.

Neural network nowadays is widely investigated in pattern recognition and signal processing fields [17]–[20]. In Scribner's proposed NN-NUC method [10], a retina-like neural network consisting of linear neuron nodes with corrected gain $G_{ij}(n)$ and corrected offset $O_{ij}(n)$ is designed to calibrate the nonuniformity response of observation $Y_{ij}(n)$ and obtain the estimation of actual response as

$$\hat{X}_{ij}(n) = G_{ij}(n) \cdot Y_{ij}(n) + O_{ij}(n) \tag{1}$$

According to the steepest descent algorithm, NN-NUC method minimizes the square error function defined in following Eq. (2) and feed back to the neural network.

$$E_{ij}(n) = \left[\hat{X}_{ij}(n) - T_{ij}(n)\right]^2 \tag{2}$$

where $T_{ij}(n)$ is the desired target image, n stands for the frame index.

However, ghosting artifacts and over-smooth effects resulted from the sudden deceleration of scene motion as well as the slow convergence rate due to the inadequate regulation of learning rate that degrade the correction performance of NN-NUC method seriously [21]. In order to suppress ghosting artifacts and eliminate the over-smooth effects with fast convergence, we present a novel scene adaptive NUC algorithm in this paper. Specifically, the proposed NUC method employs the bilateral total variation [22] penalty to optimally solve the overfitting problem. Moreover, a spatiotemporal

feature based adaptive learning rate is presented to suppress the ghosting artifacts and over-smooth effects as well as accelerate the convergence. Besides, random projection is introduced to optimize the bilateral filter and produce more accurate target value to retain more high frequency details in the correction results.

The remainder of this paper is organized as follows. The principle of the proposed algorithm is detailed in Section 2. Experimental results that illustrate the performance of the algorithm with artificial corrupted sequences and real world sequences are presented and analyzed in Section 3. Finally, discussions and conclusions are provided in Section 4.

II. METHODOLOGY

A. SCHEME DESCRIPTION

In order to deal with the overfitting problem and pick a more accurate solution, an additional regularization term is introduced in our proposed NUC method. And then the objective function can be expressed as

$$J_{ij}(n) = E_{ij}(n) + \lambda \cdot \Upsilon(\hat{X}_{ij}(n)) \tag{3}$$

where the square error function E_{ij} acts as a fidelity term to prevent pattern distortion. The parameter λ is a scalar for properly weighting the fidelity term against the regularization term $\Upsilon(\hat{X}_{ij}(n))$.

To minimize the objective function $J_{ij}(n)$, the steepest descent algorithm is used to search the optimum solution. The iterative formulas of the correction parameters are

$$G_{ij}(n+1) = G_{ij}(n) + \mu_{ij}(n) \cdot D_G\left(J_{ij}(n)\right) \tag{4}$$

$$O_{ij}(n+1) = O_{ij}(n) + \mu_{ij}(n) \cdot D_O\left(J_{ij}(n)\right) \tag{5}$$

where $\mu_{ij}(n)$ indicates the learning rate, $D_G(\cdot)$ and $D_O(\cdot)$ respectively denote the partial derivative operation applied to the gain and offset correction parameter and are represented as

$$D_G\left(J_{ij}(n)\right) = \left\{F_{ij}(n) + \lambda \cdot R_{ij}(n)\right\} \cdot Y_{ij}(n) \tag{6}$$

$$D_O\left(J_{ij}(n)\right) = \left\{F_{ij}(n) + \lambda \cdot R_{ij}(n)\right\} \tag{7}$$

where $R_{ij}(n)$ indicates the derivative of regularization term, and $F_{ij}(n)$ represents the derivative of fidelity term calculated by

$$F_{ij}(n) = \hat{X}_{ij}(n) - T_{ij}(n) \tag{8}$$

In traditional NUC methods, the learning rate is either a fixed global parameter for the whole correction process or a variable still struggle to keep up with the change of scene, which results in the slow convergence rate accompanied with ghost artifacts and over-smooth effects. In this paper, a spatiotemporal features based adaptive learning rate was proposed to enhance the adaptability and agility of the correction. Moreover, the desired target value is estimated by an innovative random projection based bilateral filter (RPBF), which effectively solves the details loss caused by the mean filter of NN-NUC method. According to the afore-described theory, the complete scheme representing the whole process of the proposed NUC method is presented in Figure 1.

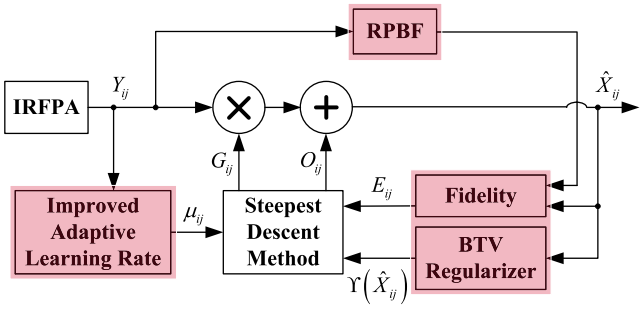

FIGURE 1. Scheme of the proposed NUC method.

B. BILATERAL TOTAL VARIATION REGULARIZER

Total variation (TV) method is one of the most popular regularization methods for image processing [23], [24]. However, TV regularizer generally leads to the staircase effect in flat region and detail loss in texture region. In order to overcome the inherent defects of the TV regularizer, a spatially adaptive regularizer called bilateral total variation (BTV) based on the spirit of the bilateral filter [25] is presented to suppress the artifacts and promote the structure preserving performance without affording a heavy computational load. The BTV regularizer is defined as

$$\Upsilon_{BTV}(\hat{X}(n)) = \underbrace{\sum_{l=-P}^{P}\sum_{m=0}^{P}}_{l+m\geq 0} \alpha^{|m|+|l|} \left\| \hat{X}(n) - S_x^l S_y^m \hat{X}(n) \right\|_1 \tag{9}$$

where S_x^l and S_y^m represent the operations of shifting $\hat{X}$ by l and m pixels in horizontal and vertical directions, respectively. The scalar weight $\alpha(0 < \alpha < 1)$ is applied to give spatially decaying effect to the summation of the regularization terms, P is the radius of the search window.

According to the objective function in Eq.(3), we introduce the BTV penalty to be the regularization term. Followed that the correction parameters solved by the steepest descent method are expressed as Eq. (6) and Eq.(7), in which the derivative of BTV regularizer is represented as

$$R_{ij}(n) = \underbrace{\sum_{l=-P}^{P}\sum_{m=0}^{P}}_{l+m\geq 0} \alpha^{|m|+|l|} \cdot \left[I - S_x^{-l} S_y^{-m}\right] \cdot sign\left(\hat{X}_{ij}(n) - S_x^l S_y^m \hat{X}_{ij}(n)\right) \tag{10}$$

where S_x^{-l} and S_y^{-m} define as the transpose of matrices S_x^l and S_y^m, respectively, and $sign(\cdot)$ is a symbolic function, I indicates the identity matrix.

C. IMPROVED ADAPTIVE LEARNING RATE

The fixed learning rate generally leads to over-smooth effects and ghosting artifacts when the scene motion is insufficient. Therefore, many kinds of adaptive learning strategies were proposed to promote the precision of the correction and

decrease the scene data dependence [26]. However, spatiotemporal information contained in the image sequence is still inadequately exploited and fused in the learning strategy [27]. In view of this, we further extract the spatiotemporal feature and present an innovative adaptive learning rate defined as

$$\mu_{ij}(n) = k_{st} \cdot \frac{\sigma_{ij}^{T}(n)}{1 + \sigma_{ij}^{S}(n)} \tag{11}$$

where k_{st} is the spatiotemporal constant, $\sigma_{ij}^{S}(n)$ is the local spatial standard deviation of the input image $Y_{ij}(n)$, and the fluctuation of error function in temporal domain is quantified by

$$\sigma_{ij}^{T}(n) = D\left[\nabla E_{ij}(n), \nabla E_{ij}(n-1), \ldots, \nabla E_{ij}(n-m+1)\right] \tag{12}$$

where m is the temporal parameter, $D[\cdot]$ indicates the standard deviation operation. The gradient of error function can be define as

$$\nabla E_{ij}(n) = E_{ij}(n) - E_{ij}(n-1) \tag{13}$$

In this spatiotemporal learning strategy, the learning rate depends on both of the spatial domain and temporal domain features. As for the contributions of temporal domain features, we can comprehend the mechanism via the following situations. With the faster scene movement, the increased fluctuation of error function would increase the learning rate and bring a faster tracking. On the contrary, the leaning rate drops to nearly zero when the scene motion paused.

As for the spatial domain features, in dynamic regions with high spatial variance that means the high frequency details need to be preserved, the corresponding learning rate should assume a smaller value. Instead, higher learning rate is taken in flat image regions to boost the convergence speed.

The abovementioned adaptive learning rate strategy significantly declines the over-smooth effects, suppresses the ghosting artifacts and accelerates the convergence speed.

D. BILATERAL FILTER WITH RANDOM PROJECTION

Traditional NN-NUC methods adopt the local mean filtering approach to obtain the desired target image. However, the mean filter tends to smooth the textures and produce blurry corrected results [28]. In view of this, Rossi and Diani [29] employed bilateral filter (BF) to acquire more accurate target value and suppress the nonuniformity. Random projection [30] approach containing the thought of dimension reduction [31] is successfully introduced to promote the accuracy and reduce the computational load of the nonlocal means filter in [32]. Motivated by the abovementioned ideas, we proposed a random projection based bilateral filter (RPBF) to obtain more accurate desired target image. Since accurate target image is benefit for preserving the edges and details in the corrected image, the proposed RPBF will undoubtedly contribute to the promotion of correction precision.

In RPBF, we introduce random projection to perform dimension reduction for each neighborhood vector. As for the random projection process, the $d \times d$ patch with the center of (i, j) in the observation Y is projected to a $l \times d$ dimensional subspace by using a $l \times d$ random matrix R, which is formulated as

$$f_{l\times d}^{PR}(i,j) = R_{l\times d} \cdot Y_{d\times d}(i,j) \tag{14}$$

According to the afore-described theory, the desired image acquired by RPBF ($l = 1$) can be defined as

$$T(i,j) = \frac{\sum_{k=-d}^{d} f_{1\times d}^{PR}(i, j+k) \cdot w_s(i,k) \cdot w_r(i,k)}{\sum_{k=-d}^{d} w_s(i,k) \cdot w_r(i,k)} \tag{15}$$

where $w_s(i,k)$ and $w_r(i,k)$ respectively denote the spatial weight and range weight and are defined as

$$w_s(i,k) = \exp\left(-\frac{k^2}{2\sigma_s^2}\right) \tag{16}$$

$$w_r(i,k) = \exp\left(-\frac{\left\|f_{1\times d}^{PR}(i,j) - f_{1\times d}^{PR}(i,j+k)\right\|^2}{2\sigma_r^2}\right) \tag{17}$$

where σ_s and σ_r are the smooth parameters controlling the decay of the two weight factors.

III. EXPERIMENTAL RESULTS AND ANALYSIS

In this section, several experiments were performed to compare the performance of the proposed NUC method with NN-NUC [10], FA-NUC [26] and TV-NUC [33] on artificially corrupted sequences and real infrared sequence, respectively. In order to perform the comprehensive performance verification, the proposed RPBF and traditional BF are employed to generate the desired image in the proposed NUC method so called BTV+RPBF and BTV+BF, respectively. For each NUC method, we initialize the corrected gain $G_{ij}(0)$ and offset $O_{ij}(0)$ with one and zero for each neural node, respectively. In all of the following experiments, the learning rates are fine-tuned to pursuit the best performance with a trade-off between convergence speed and stability.

A. PARAMETER SENSITIVITY ANALYSIS

In this simulation, the sensitivity analysis of the hyper parameters will be conducted on different selections of the spatial weight α and the balance scalar λ. The goal is to find out the optimum configuration of α and λ for seeking the optimal performance of the proposed NUC method and further give the corresponding theoretical explanation. The PSNR curves of different selection of α and λ are shown in Figure 2. By comparing with the relevant results, we can clearly find that higher spatial weight yields faster convergence rate but with more instability, while balanced scalar is help to achieve satisfied performance. Moreover, different combinations of α and λ produce varied convergence rate but nearly coincide to similar PSNR after 1300 frames of iterations.

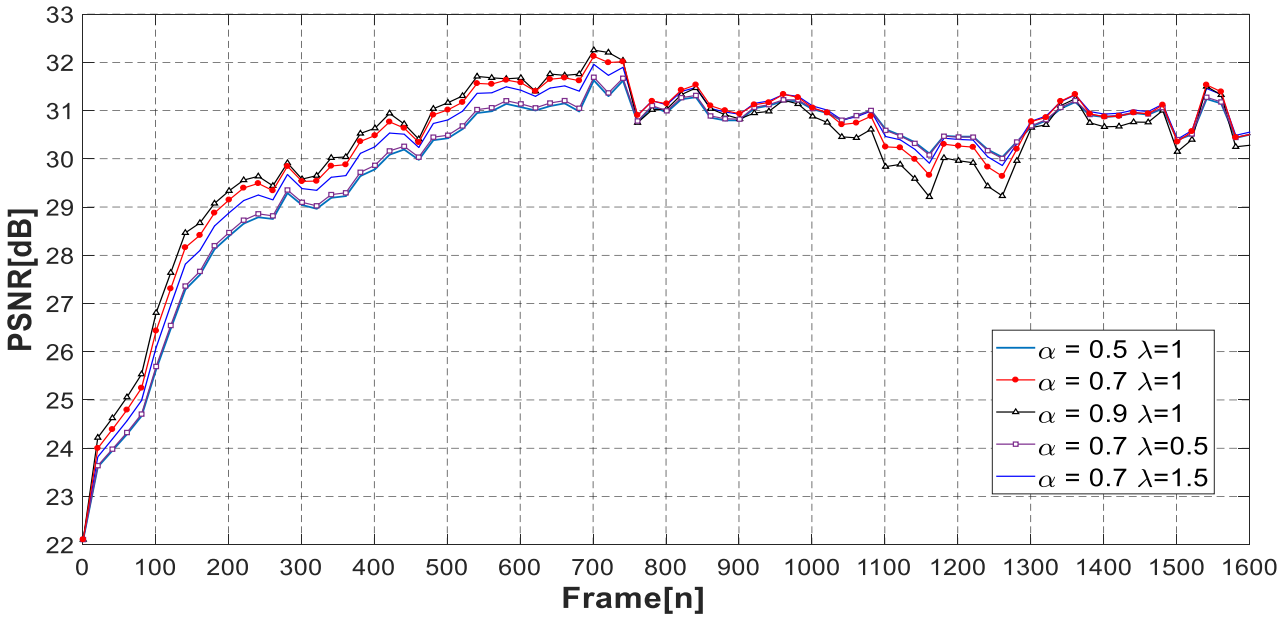

FIGURE 2. Correction performance of various parameter selections for the proposed NUC method.

In terms of principle, α acts as a spatial weight for different scales of derivatives, larger α considers a larger neighborhood, but a too large α may remove the point like details from the image as the TV prior do and causes more undesired smoothing. In contrast, a too small α prefers to sharply decay the weight with the expansion of neighborhood, which weakens the noise reduction performance and causes slower convergence. As for the balance scalar λ, a larger λ increases the impact of regularizer and gives rise to agile tracking, while a smaller λ tends to stress the regularizer and provides stable convergence.

According to the abovementioned analysis, we can find that a proper selection of α yields satisfied noise reduction effect and an appropriate assignment of λ balances the stability and agility. In general, the selection margin for α and λ is sufficient, which reduces the difficulty of parameter tuning.

B. PERFORMANCE ASSESSMENT WITH SIMULATED SEQUENCES

In this section, two infrared sequences corrupted by artificial fixed pattern noise are employed to evaluate the performance of different NUC methods. Sequence 1 consists of 1600 frames of 512 × 384 sized infrared images collected from RTD3172C imager (IRay, Yantai, China). Sequence 2 consists of 4000 frames of 471 × 358 sized images collected by A615 camera (FLIR Systems, Inc., Wilsonville, OR, USA). To simulate the nonuniform response of the detectors, the stripe gain noise with mean 1 and standard deviation 0.15 as well as offset noise with mean 0 and standard deviation 12 generated as realizations of independent and identically distributed (iid) Gaussian random variables are applied to both of sequence 1 and sequence 2.

In the following experiments, PSNR [34] and roughness index [35] are utilized to assess the quality of the final corrected image. The roughness index can be calculated by

$$\rho = \frac{\left\| h_1 \otimes \hat{X} \right\|_1 + \left\| h_2 \otimes \hat{X} \right\|_1}{\left\| \hat{X} \right\|_1} \tag{18}$$

where h_1 is the horizon vector and be set as $[1, -1]$, and $h_2 = h_1^T$ is the vertical vector. The operator $\|\cdot\|_1$ indicates the L1-norm.

1) ANALYSIS OF CORRECTION ACCURACY AND CONVERGENCE RATE

Figure 3 presents the correction performance of each nuc methods upon artificially corrupted sequence 1. from Figure 3(a), we can find that both of the psnr curves of btV+RPbf and btV+Bf method converge faster and take the lead to reach a higher level. moreover, the btV+RPbf method achieves nearly 0.8db promotion over btV+Bf method, which is benefited from the much richer details preserved in the desired target image by using the proposed rpbf. as can be seen clearly from the roughness curves plotted in Figure 3(b), the proposed btV+RPbf method obtains lower roughness value. even though tv-nuc converges faster than btV+Bf method in the former 400 frames, the btV+Bf method obtains lower roughness in the rest of the sequence, this fact indicates that the corrected results of our proposed nuc method remove the fpn noise more efficiently.

Performance assessed with average PSNR and roughness of each entire correction processes are listed in Table 1, where the proposed BTV regularized NUC methods (including BTV+BF and BTV+RPBF method) outperform the existing NN-NUC, FA-NUC and TV-NUC. In addition, the proposed

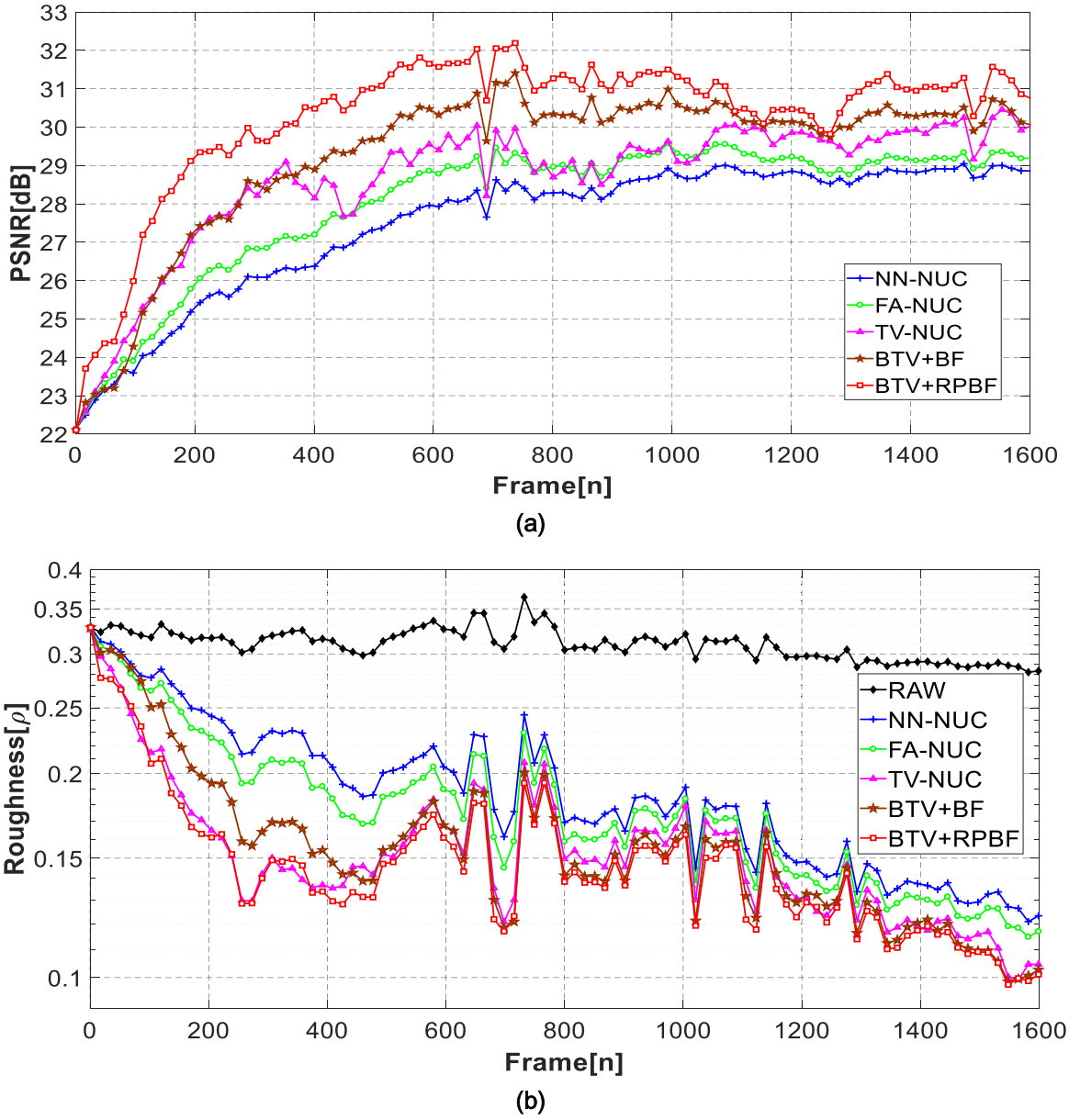

FIGURE 3. Correction performance of various NUC methods for artificially corrupted sequence 1. (a) PSNR (dB) and (b) Roughness (ρ).

TABLE 1. Mean psnr and roughness index for sequence 1.

Metrics	Corrupted Image	Corrected Image				
		NN-NUC	FA-NUC	TV-NUC	BTV+BF	BTV+RPBF
PSNR(dB)	21.69	27.62	28.16	28.80	29.37	30.09
Roughness Index (ρ)	0.3083	0.1833	0.1751	0.1521	0.1513	0.1494

BTV+RPBF method obtains obvious improvement in both of PSNR and roughness index, which validates the joint contributions of the BTV regularization and RPBF approach for the promotion of correction accuracy.

2) COMPARISON OF DEGHOSTING PERFORMANCE

In this section, the deghosting performance of different NUC methods is verified with artificially corrupted sequence 2. Figure 4 shows that the proposed BTV+RPBF and BTV+BF method grow faster and achieve higher PSNR. For the TV-NUC method, the PSNR curve keeps a slow increase during the first 900 frames. Thereafter, the performance promotion of the TV-NUC shows large fluctuation in PSNR. The main reason is that the TV-NUC is very sensitive to the frequent scene switching, which sometimes interrupts and restarts the convergence process.

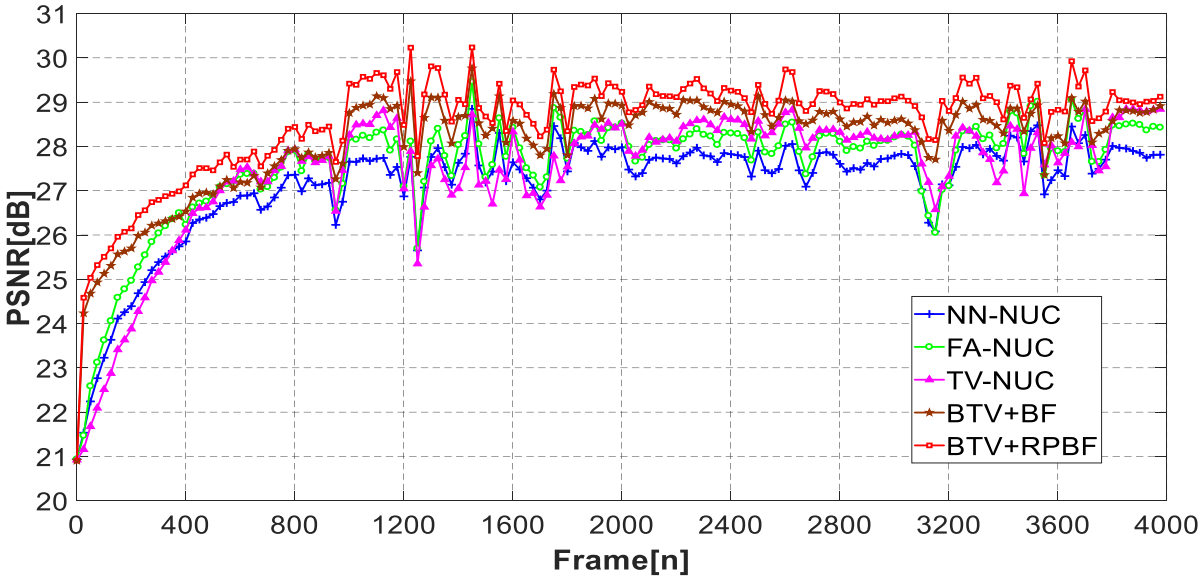

FIGURE 4. PSNR curves of various NUC methods for artificially corrupted sequence 2.

TABLE 2. Mean psnr and roughness index for sequence 2.

Metrics	Corrupted Image	Corrected Image				
		NN-NUC	FA-NUC	TV-NUC	BTV+BF	BTV+RPBF
PSNR(dB)	20.17	27.18	27.56	27.48	28.15	28.42
Roughness Index (ρ)	0.2777	0.1198	0.1144	0.1193	0.1132	0.1076

Figure 5 shows the visual effects of various NUC methods for 1210th frame (motion restarted after the halt) of sequence 2. Figure 5(b)-(f) shows the corrected results using the NN-NUC, FA-NUC, TV-NUC, BTV+BF and BTV+RPBF method, respectively. From Figure 5(b)-(c), we can clearly observe serious ghosting artifacts in the NN-NUC results and FA-NUC results, which resulted from the inaccurate estimation of desired image by using local mean filter. In view of this, the TV-NUC suppresses the ghosting artifacts by minimizing the TV of the estimated irradiance but resides amount of nonuniformity for its sensitivity of scene switching. In contrast, our proposed BTV+BF and BTV+RPBF method estimate the desired image with more accurate spatial filter named BF and RPBF, and then employ BTV penalty to produce a more optimal estimation of correction parameters, furthermore, present a spatiotemporal feature based adaptive learning rate to agilely track the scene change and suppress the ghosting artifact more effectively. The visual effect presented in Figure 5(e) shows that BTV+BF method reduces most of the ghosting artifacts as well as eliminates the nonuniformity obviously. As shown in Figure 5(f), BTV+RPBF method can further promote the deghosting performance for the substitution of BF with proposed RPBF.

The mean PSNR and roughness index of the whole iterative process are shown in Table 2. It is worth to note that the PSNR of the TV-NUC doesn't exceed FA-NUC due to the frequently scene switching. FA-NUC method gains better deghosting performance than NN-NUC by employing adaptive learning rate strategy to update the correction parameters swiftly. Similar with the experimental results of sequence 1, the proposed BTV+RPBF method obtains the highest PSNR and smallest roughness index, and this further proves the outstanding performance in both of ghosting suppression and nonuniformity correction.

C. APPLICATION TO REAL INFRARED IMAGE SEQUENCE

In order to evaluate the practical performance of the proposed method, 1970 frames of real infrared data (named sequence 3) collected by a 384 × 288 ULIS Pico384 camera (ULIS, Veurey-Voroize, France). In these experiments, the roughness index is employed to illuminate the nonuniformity correction performance of varies NUC methods. Note that, only the roughness index cannot assess the correction performance integrally. In the normal NUC process, the roughness index of the corrected image will decrease to a proper level, extremely small roughness index indicates the image is over-smooth. Therefore, we consider the over-smooth suppression as well as nonuniformity elimination and deghosting in the performance assessment.

1) COMPARISON OF OVER-SMOOTH SUPPRESSION

To verify the over-smooth suppression capability after the scene motion paused (from 940th frame to 1110th frame), we apply various NUC methods upon sequence 3 and plot the roughness curves of the correction results in the Figure 6. It is worthy of note that the roughness curves of NN-NUC,

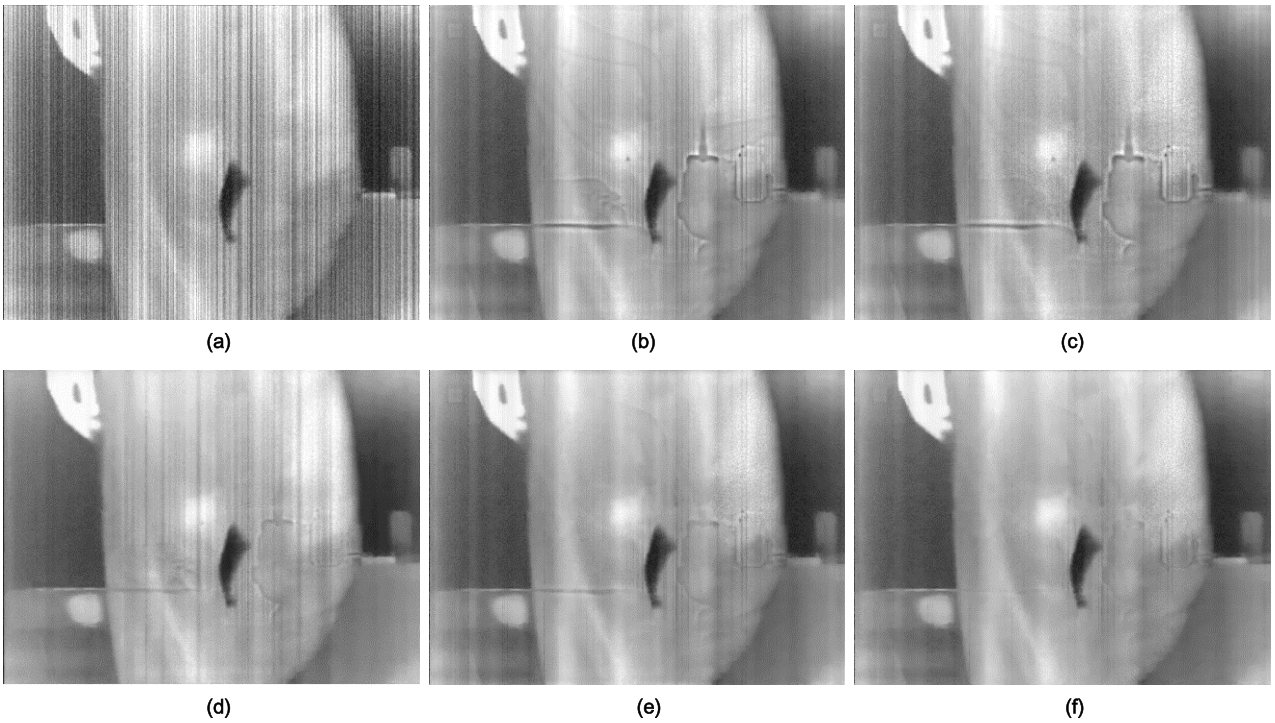

FIGURE 5. Visual effect of corrected results for 1210th frame in sequence 2. (a) Corrupted image; (b) Corrected results of NN-NUC; (c) Corrected results of FA-NUC; (d) Corrected results of TV-NUC; (e) Corrected results of BTV+BF; (f) Corrected results of BTV+RPBF.

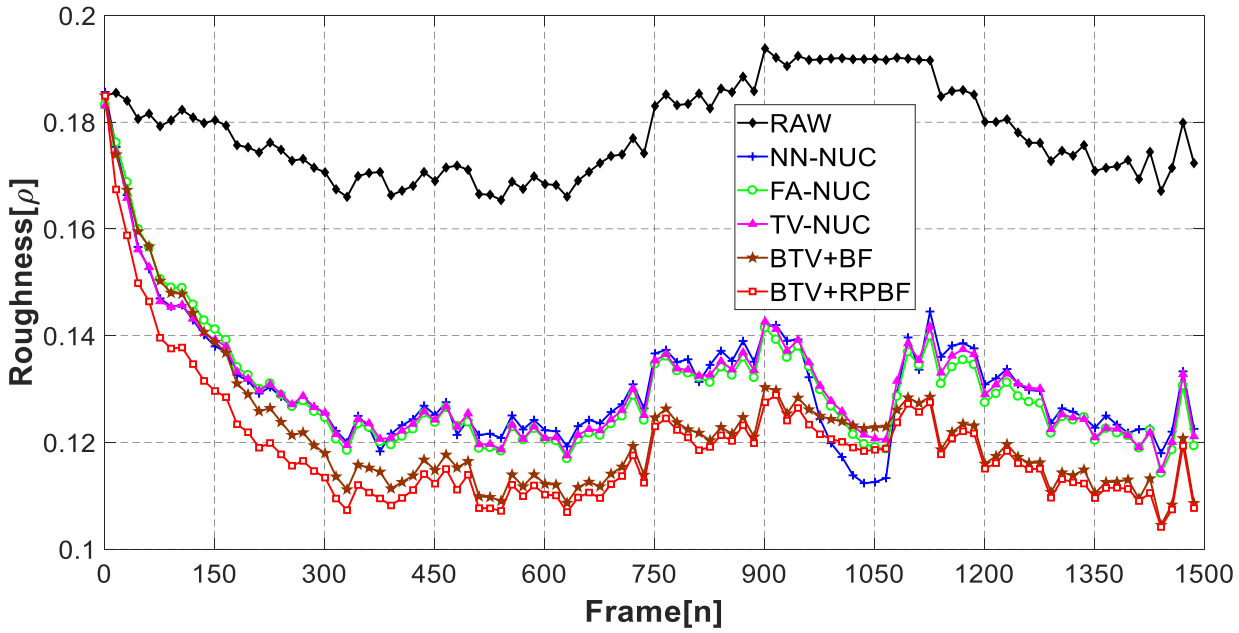

FIGURE 6. The roughness index curves of sequence 3.

FA-NUC and TV-NUC all sharply descend and reach a concave point, which indicates these methods still implement high strength correction even in pause stage and produce over-smooth image (this phenomenon can be observed in Figure 8(b)-(d)). In contrast, the roughness curves of our proposed method change comparatively gently in halt stage, which demonstrates the proposed method avoiding the over-smooth effects more successfully.

In order to further evaluate the effectiveness of the proposed adaptive learning rate strategy in over-smooth suppression, the learning rate curves of FA-NUC and the proposed method are compared in Figure 7 to show the self-regulation ability. Accordingly, NN-NUC and TV-NUC with fixed learning rate are not included into comparison. As shown in Figure 7, the FA-NUC method adjusts the learning rate slightly and relieves the over-smooth effects to a certain

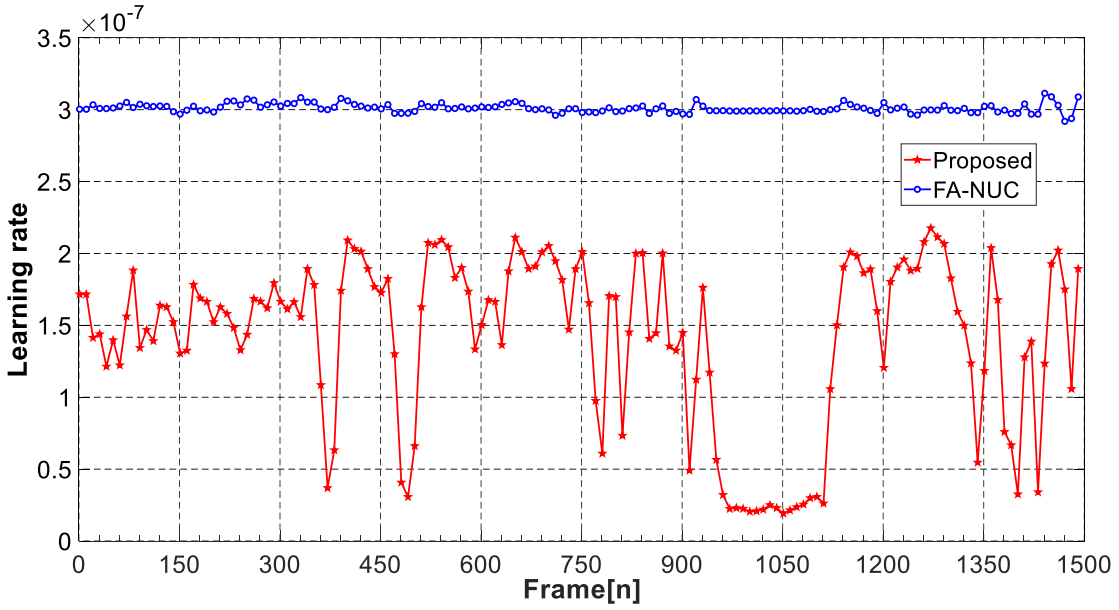

FIGURE 7. The learning rate curves of FA-NUC and the proposed method.

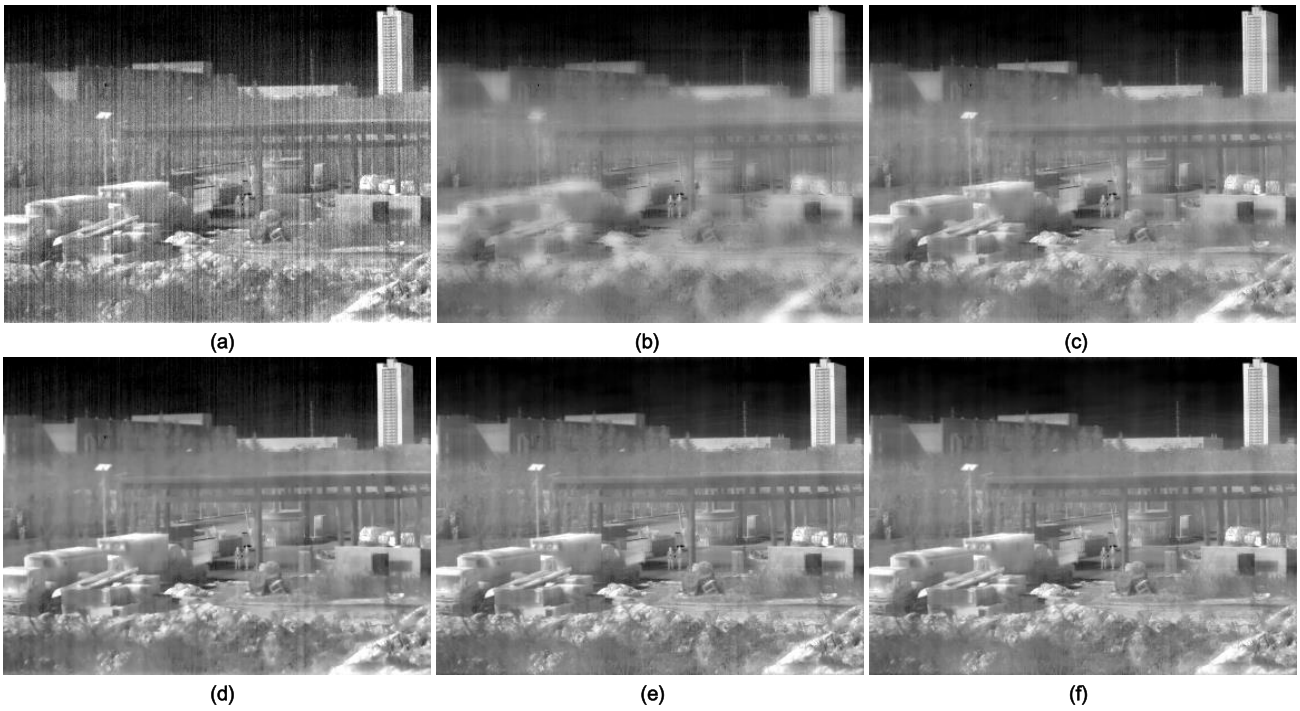

FIGURE 8. Corrected results of varies NUC method of 1046th frame in sequence 3. (a) Raw image; (b) Corrected results of NN-NUC; (c) Corrected results of FA-NUC; (d) Corrected results of TV-NUC; (e) Corrected results of BTV+BF; (f) Corrected results of BTV+RPBF.

extent. By contrast, our proposed adaptive learning rate performs better adaptability, which rapidly decreases nearly to zero and almost suspends the update of correction parameters in the scene motionless stage.

In addition, the subjective visual effects of the corrected 1046th image (a frame in a halt of sequence 3) are introduced to assess the effectiveness of the abovementioned NUC methods. The corrected results of NN-NUC, FA-NUC, TV-NUC, BTV+BF and BTV+RPBF are shown in Figure 8(b)-(f), respectively. It can be seen clearly that NN-NUC method produces the most serious over-smooth results and FA-NUC method preserves most of the obvious edges but still damages the textures severely. The TV-NUC method further suppresses the over-smooth effects but fails in the discrimination of details and residual nonuniformity. As for our proposed BTV+BF and BTV+RPBF method, the corrected results simultaneously preserve rich high-frequency details and remove the nonuniformity more thoroughly.

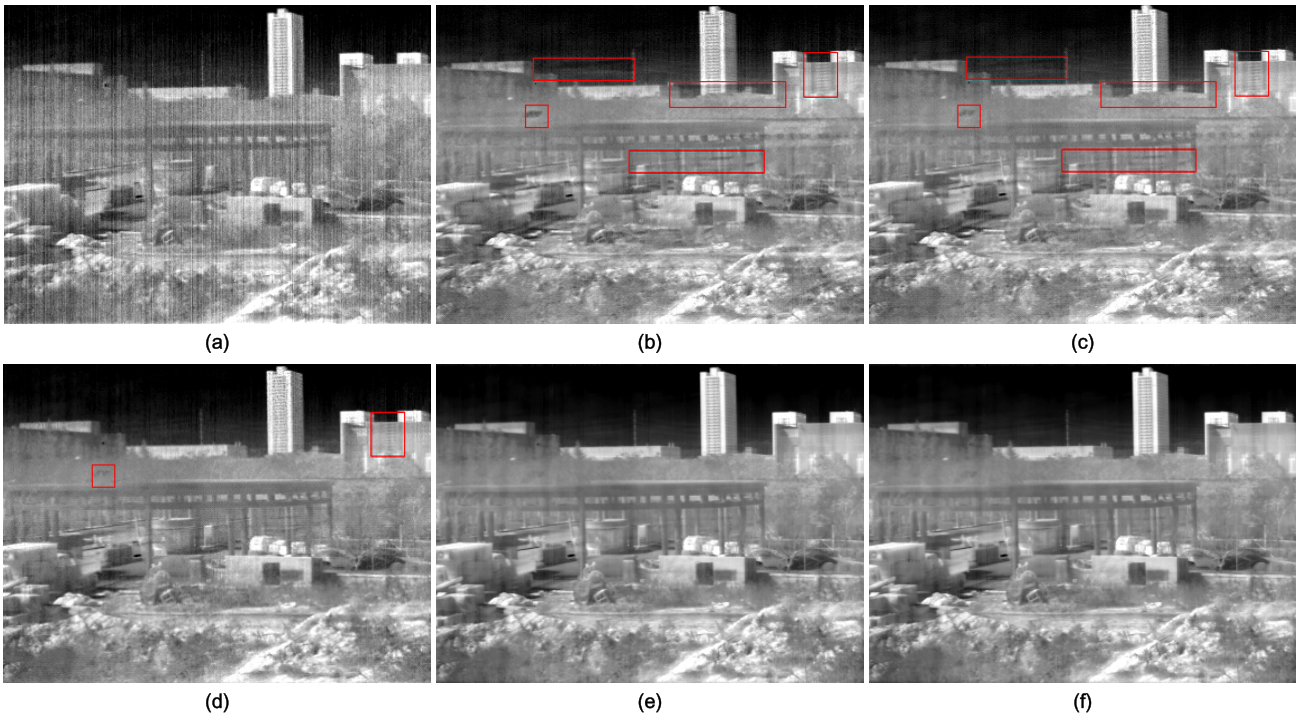

FIGURE 9. Corrected results of varies NUC method of 1155th frame in sequence 3. (a) Raw image; (b) Corrected results of NN-NUC; (c) Corrected results of FA-NUC; (d) Corrected results of TV-NUC; (e) Corrected results of BTV+BF; (f) Corrected results of BTV+RPBF.

2) COMPARISON OF DEGHOSTING EFFECT

After the scene motion resumed (after 1110th frame), the NN-NUC method produces serious ghosting artifacts for the following 50 frames at least (this phenomenon could be observed in the following Figure 9(b)). Note that the learning rate of the proposed method in Figure 7 recovers immediately after the resume of scene motion. The larger learning rate updates the correction parameters quickly to adapt to the switching scene. By this way, our proposed learning rate strategy can suppress the ghosting artifacts well.

In order to observe the ghosting artifacts, the 1155th frame in sequence 3 is used as an example. As can be seen in Figure 9, the NN-NUC and the FA-NUC suffer from serious ghosting artifacts marked out by red boxes. The TV-NUC method suppresses partial ghosting artifacts while letting a certain amount of residual nonuniformity off (existed especially on the highest building and sky region in Figure 9(d)). The proposed BTV+BF and BTV+RPBF eliminate the nonuniformity thoroughly and pay same attention to ghost suppression, which is validated by the sharply visual effect of Figure 9(e) and (f).

IV. CONCLUSIONS

While many scene adaptive NUC approaches had been presented to suppress the FPN in the infrared images, they are not able to solve the ghosting artifacts accompanied with over-smooth effects. To this end, we introduce a BTV penalty into the objective function to reduce the ghosting artifacts as well as suppress nonuniformity response, and then present a spatiotemporal adaptive learning rate strategy to further remove the ghost, eliminate the over-smooth effect and accelerate the convergence rate. Moreover, random projection based bilateral filter is proposed to preserve the details in the corrected images. Experiments with both of simulated data and real scene have demonstrated that the proposed NUC method achieves higher correction precision with faster convergence rate. In addition, the correction results of our proposed method have a sharper visual effect without perceptible ghosting artifacts and over-smooth effects.

REFERENCES

[1] L. Du *et al.*, "A reconfigurable streaming deep convolutional neural network accelerator for Internet of Things," *IEEE Trans. Circuits Syst. I, Reg. Papers*, vol. 65, no. 1, pp. 198–208, Aug. 2017.

[2] L. Liu, C. Chen, T. Qiu, M. Zhang, S. Li, and B. Zhou, "A data dissemination scheme based on clustering and probabilistic broadcasting in VANETs," *Veh. Commun.*, vol. 13, pp. 78–88, Jul. 2018.

[3] W. Tan, C. Zhao, and H. Wu, "Intelligent alerting for fruit-melon lesion image based on momentum deep learning," *Multimedia Tools Appl.*, vol. 75, no. 24, pp. 16741–16761, Dec. 2016.

[4] M. Lopez-Martin, B. Carro, A. Sanchez-Esguevillas, and J. Lloret, "Network traffic classifier with convolutional and recurrent neural networks for Internet of Things," *IEEE Access*, vol. 5, pp. 18042–18050, 2017.

[5] C. Chen, L. Liu, T. Qiu, K. Yang, F. Gong, and H. Song, "ASGR: An artificial spider-Web-based geographic routing in heterogeneous vehicular networks," *IEEE Trans. Intell. Transp. Syst.*, to be published, doi: 10.1109/TITS.2018.2828025.

[6] K. Liang, C. Yang, L. Peng, and B. Zhou, "Nonuniformity correction based on focal plane array temperature in uncooled long-wave infrared cameras without a shutter," *Appl. Opt.*, vol. 56, no. 4, pp. 884–889, Feb. 2017.

[7] A. Jara *et al.*, "Joint de-blurring and nonuniformity correction method for infrared microscopy imaging," *Infr. Phys. Technol.*, vol. 90, pp. 199–206, May 2018.

[8] F. Fan, Y. Ma, J. Huang, Z. Liu, and C. Liu, "A combined temporal and spatial deghosting technique in scene based nonuniformity correction," *Infr. Phys. Technol.*, vol. 71, pp. 408–415, Jul. 2015.

[9] A. Friedenberg and I. Goldblatt, "Nonuniformity two-point linear correction errors in infrared focal plane arrays," *Opt. Eng.*, vol. 37, no. 4, pp. 1251–1254, Apr. 1998.
[10] D. A. Scribner *et al.*, "Adaptive retina-like preprocessing for imaging detector arrays," in *Proc. IEEE Int. Conf. Neural Netw.*, vol. 3, 1993, pp. 1955–1960.
[11] Z. Liu, Y. Ma, F. Fan, and J. Ma, "Nonuniformity correction based on adaptive sparse representation using joint local and global constraints based learning rate," *IEEE Access*, vol. 6, pp. 10822–10839, 2018.
[12] H. Yu, Z.-J. Zhang, and C.-S. Wang, "An improved retina-like nonuniformity correction for infrared focal-plane array," *Infr. Phys. Technol.*, vol. 73, pp. 62–72, Nov. 2015.
[13] W. Qian, Q. Chen, and G. Gu, "Space low-pass and temporal high-pass nonuniformity correction algorithm," *Opt. Rev.*, vol. 17, no. 1, pp. 24–29, Jan. 2010.
[14] S. Rong, H. Zhou, D. Zhao, K. Cheng, K. Qian, and H. Qin, "Infrared fix pattern noise reduction method based on Shearlet Transform," *Infr. Phys. Technol.*, vol. 91, pp. 243–249, Jun. 2018.
[15] H.-B. Leng, B.-L. Hu, Z.-F. Zhou, L.-N. Tang, J. Zhang, and A.-Q. Yan, "Adaptive nonuniformity correction algorithm based on multiscale temporal moment matching," *J. Infr. Millim. Waves*, vol. 34, no. 4, pp. 401–405, Aug. 2015.
[16] J. G. Harris and Y.-M. Chiang, "Nonuniformity correction of infrared image sequences using the constant-statistics constraint," *IEEE Trans. Image Process.*, vol. 8, no. 8, pp. 1148–1151, Aug. 1999.
[17] C. Chen, X. Liu, H.-H. Chen, M. Li, and L. Zhao, "A rear-end collision risk evaluation and control scheme using a Bayesian network model," *IEEE Trans. Intell. Transp. Syst.*, to be published, doi: 10.1109/TITS.2018.2813364.
[18] H. Luo, Y. Yang, B. Tong, F. Wu, and B. Fan, "Traffic sign recognition using a multi-task convolutional neural network," *IEEE Trans. Intell. Transp. Syst.*, vol. 19, no. 4, pp. 1100–1111, Apr. 2018.
[19] Q. Liu and H. Leung, "Variable Augmented Neural Network for Decolorization and Multi-Exposure Fusion," *Inf. Fusion*, vol. 46, pp. 114–127, Mar. 2019.
[20] K. Park, S. Yu, S. Park, S. Lee, and J. Paik, "An optimal low dynamic range image generation method using a neural network," *IEEE Trans. Consum. Electron.*, vol. 64, no. 1, pp. 69–76, Feb. 2018.
[21] L. Rui, Y. Yin-Tang, Z. Duan, and L. Yue-Jin, "Improved neural network based scene-adaptive nonuniformity correction method for infrared focal plane arrays," *Appl. Opt.*, vol. 47, no. 24, pp. 4331–4335, Aug. 2008.
[22] S. Farsiu, M. D. Robinson, M. Elad, and P. Milanfar, "Fast and robust multiframe super resolution," *IEEE Trans. Image Process.*, vol. 13, no. 10, pp. 1327–1344, Oct. 2004.
[23] L. I. Rudin, S. Osher, and E. Fatemi, "Nonlinear total variation based noise removal algorithms," *Phys. D, Nonlinear Phenomena*, vol. 60, nos. 1–4, pp. 259–268, 1992.
[24] A. Beck and M. Teboulle, "Fast gradient-based algorithms for constrained total variation image denoising and deblurring problems," *IEEE Trans. Image Process.*, vol. 18, no. 11, pp. 2419–2434, Nov. 2009.
[25] C. Tomasi and R. Manduchi, "Bilateral filtering for gray and color images," in *Proc. IEEE 6th Int. Conf. Comput. Vis.*, Bombay, India, Jan. 1998, pp. 836–846.
[26] E. Vera and S. Torres, "Fast adaptive nonuniformity correction for infrared focal-plane array detectors," *EURASIP J. Adv. Signal Process.*, vol. 13, Dec. 2005, Art. no. 560759.
[27] H. Zhu *et al.*, "YoTube: Searching action proposal via recurrent and static regression networks," *IEEE Trans. Image Process.*, vol. 27, no. 6, pp. 2609–2622, Jun. 2018.
[28] R. Sheng-Hui, Z. Hui-Xin, Q. Han-Lin, L. Rui, and Q. Kun, "Guided filter and adaptive learning rate based non-uniformity correction algorithm for infrared focal plane array," *Infr. Phys. Technol.*, vol. 76, pp. 691–697, May 2016.
[29] A. Rossi, M. Diani, and G. Corsini, "Bilateral filter-based adaptive nonuniformity correction for infrared focal-plane array systems," *Opt. Eng.*, vol. 49, no. 5, pp. 57003–57013, May 2010.
[30] E. Bingham and H. Mannila, "Random projection in dimensionality reduction: Applications to image and text data," in *Proc. ACM Int. Conf. Knowl. Discovery Data Mining.*, San Francisco, CA, USA, 2001, pp. 245–250.
[31] Z. Huang, H. Zhu, J. T. Zhou, and X. Peng, "Multiple marginal Fisher analysis," *IEEE Trans. Ind. Electron.*, to be published, doi: 10.1109/TIE.2018.2870413.
[32] R. Lai and Y. T. Yang, "Accelerating non-local means algorithm with random projection," *Electron. Lett.*, vol. 47, no. 3, pp. 182–183, Feb. 2011.
[33] E. Vera, P. Meza, and S. Torres, "Total variation approach for adaptive nonuniformity correction in focal-plane arrays," *Opt. Lett.*, vol. 36, no. 2, pp. 172–174, 2011.
[34] Y. A. Y. Ai-Najjar and D. C. Soong, "Comparison of image quality assessment: PSNR, HVS, SSIM, UIQI," *Int. J. Sci. Eng. Res.*, vol. 3, no. 8, pp. 1–5, Aug. 2012.
[35] M. M. Hayat, S. N. Torres, E. Armstrong, S. C. Cain, and B. Yasuda, "Statistical algorithm for nonuniformity correction in focal-plane arrays," *Appl. Opt.*, vol. 38, no. 5, pp. 772–780, 1999.

RUI LAI received the B.S. degree in information engineering from Xidian University, in 2002, and the M.S. and Ph.D. degrees in electronic science and technology, in 2005 and 2007, respectively.

From 2009 to 2010, he was a Postdoctoral Researcher with the Optoelectronic Science and Engineering Department, Huazhong University of Science and Technology. Since 2010, he has been an Associate Professor with the Microelectronics Department, Xidian University. He has authored more than 60 journal and conference papers. His research interests include computational photography, image sensors, image processing, and deep learning.

JUNTAO GUAN received the B.S. degree in integrated circuit design and integration system from the Harbin University of Science and Technology, in 2016. He is currently pursuing the Ph.D. degree in electronics science and technology with Xidian University, Xi'an, China.

His research interests include the application of deep learning to image analysis, infrared image process, and image sensors.

YINTANG YANG received the B.S. and M.S. degrees in semiconductor devices and microelectronics from Xidian University, Xi'an, China, in 1982 and 1984, respectively, and the Ph.D. degree in microelectronics and solid state electronics from Xi'an Jiaotong University, Xi'an, in 2000.

Since 1997, he has been a Professor of microelectronics and the Director of the Institute of Microelectronics, Xidian University. He has published three books and more than 140 journal and conference papers. His research interests include design methodologies and techniques for analog and mixed-signal CMOS integrated circuits, micromechanical system, and sensors.

Dr. Yang received the National Science Fund for Distinguished Young Scholars from the National Natural Science Foundation of China, in 2007. He served on the Editorial Board of four journals.

AI XIONG received the B.S. and M.S. degrees in automation and control theory and engineering from Chongqing University, Chongqing, in 2002 and 2005, respectively, and the Ph.D. degree in signal and information processing from the Institute of Optics and Electronics, Chinese Academy of Sciences, Chengdu, China, in 2008.

From 2008 to 2016, he was a Research Assistant with the Institute of Optics and Electronics, Chinese Academy of Sciences. Since 2016, he has been an Associate Professor with the Control Engineering College, Chengdu University of Information Technology, Chengdu. His research interests include optical sensors, high-precision servo control, and adaptive control.